FIR Analysis of Upconversion Intensity Data for Non-Contact Temperature Sensing based on Gd_2O_2S: 9% Yb^{3+}, 1% Er^{3+}

Nabin Chapagain[a], Forough Jahanbazi[b], Madhab Pokhrel[a], Yuanbing Mao[b], Amir Shahmoradi[a,c]

[a]*Department of Physics, The University of Texas, Arlington, 76010, Tx, USA*
[b]*Department of Chemistry, Illinois Institute of Technology, Chicago, 60616, Il, USA*
[c]*Division of Data Science, The University of Texas, Arlington, 76010, Tx, USA*

Abstract

The Fluorescence Intensity Ratio (FIR) of the two green emission bands resulting from $^2H_{11/2} \rightarrow ^4I_{15/2}$ and $^4S_{3/2} \rightarrow ^4I_{15/2}$ for Er^{3+} in a system of 9% Yb^{3+}, 1% Er^{3+} co-doped Gd_2O_2S nanophosphor is proposed as a model for upconversion-based non-contact temperature sensing. The nanophosphor is proposed as a well-suited material for non-contact temperature sensing due to its efficient upconversion luminescence under 980 nm excitation. The emissive intensity of the radiation, praticularly from Er^{3+} is highly temperature dependent, making it ideal for ratiometric temperature sensing.

Keywords: Upconversion, Optical Thermometry, Erbium, Fluorescence Intensity Ratio (FIR), Thermally Coupled

1. Introduction

Optical thermometry employing rare-earth ion-doped upconversion (UC) phosphors has emerged as a promising technique for non-contact temperature sensing, particularly in environments where traditional thermometry methods fail due to electromagnetic interference, high temperatures, or small measurement scales. UC phosphors, which convert lower-energy photons (typically near-infrared) into higher-energy emissions (visible or ultraviolet) [1, 2, 3], offer unique advantages such as high sensitivity, miniaturization potential, and the ability to measure temperatures with high spatial resolution in biological and industrial applications.

Among the rare earth trivalent ions, emissions from Erbium (Er^{3+}) ions are well-suited for optical thermometry [4]. Erbium's electronic states are particularly suitable for luminescence due to several key properties: Erbium (Er^{3+}) has a rich set of energy levels within its 4f electron shell. These levels are shielded by the outer 5s and 5p electrons, which minimize the interaction with the host lattice, leading to sharp optical transitions. This results in narrow emission lines with high color purity.

The transitions between the energy levels of Er^{3+}, particularly those from the excited states $^2H_{11/2}$, $^4S_{3/2}$, and $^4F_{9/2}$ to the ground state ($^4I_{15/2}$), have relatively long lifetimes. This allows for efficient controlling of population density, which is beneficial for applications like temperature sensors because luminescence intensity is a temperature-dependent phenomenon where fluorescence intensity ratio (FIR) changes linearly with temperature [5]. The FIR technique, where the ratio of the intensities of two thermally coupled levels of Er^{3+} (typically $^2H_{11/2}$ and $^4S_{3/2}$) is measured, is commonly employed for temperature sensing. The sensitivity of this method stems from the Boltzmann distribution of the population between these levels, which varies with temperature [6].

The host material compatibility also gives Er^{3+}-doped system a potential advantage as a temperature sensor since Er^{3+} can be doped into various host materials like crystals, glasses, and ceramic powders without significantly altering the luminescence wavelength. Due to the crystal field in the host material, the degenerate energy levels of Er^{3+} split into Stark levels, providing more transitions for both absorption and emission, enhancing the versatility in luminescent applications. These characteristics make Erbium a valuable dopant for luminescent materials, where its electronic states can be leveraged to increase the photon yields if doped into a suitable host, as the choice of the host can influence upconversion efficiency.

FIR is typically used to predict the temperature based on the measured intensity because of its higher sensitivity and theoretical linear relationship between the natural logarithm of FIR ($\log(R)$) and the reciprocal of temperature ($1/T$). FIR is defined as the ratio of emissions from higher to that of lower excited levels, which is done by calculating the ratio of integrated intensities for those transitions, which also includes the results of Stark effect [7, 8].

Furthermore, numerous papers discussing optical thermometry have demonstrated the performance of the phosphors up to 550 - 600 Kelvin [9, 10, 11]. However, utilizing this novel phosphor Gd_2O_2S, we experimentally recorded the luminescence data up to 875 Kelvin. Finding a host that possesses a low phonon spectral mode, while being non-toxic, chemically stable, and can be mass-produced at low cost is a challenge and has garnered a lot of attention recently.

Haase et al. [12] identifies $NaYF_4$: Yb/Er as the most efficient host material. However, Pokhrel et al. [13] show that

Email addresses: nabin.chapagain@mavs.uta.edu (Nabin Chapagain), madhab.pokhrel@uta.edu (Madhab Pokhrel), shahmoradi@utexas.edu (Amir Shahmoradi)

Yb/Er doped Y_2O_2S, La_2O_2S and Gd_2O_2S are equally or even brighter than $NaYF_4$: Yb/Er. Under low power excitation, [13] reports significant upconversion of Yb/Er doped Gd_2O_2S, indicating that the upconversion efficiency in the material is notably higher compared to other materials. This led us to use Yb/Er doped Gd_2O_2S as the host in our experiment, with the doping concentration of 9% Yb^{3+}/ 1% Er^{3+} [13].

In this work, we explore the temperature-dependent upconversion luminescence data from 9% Yb^{3+}/1 % Er^{3+}, thereby proposing more precise, reliable, and versatile temperature sensors, and discuss the challenges and potential applications for optical thermometry. By analyzing the spectral changes in upconverted luminescence with temperature, we have elucidated the mechanisms behind the thermal sensing capabilities of this particular dopant and host combination. We have demonstrated that Gd_2O_2S: Er,Yb phosphors could be used for high-temperature applications, with sensing capabilities up to 875 K.

2. Methodology

2.1. Sample Synthesis

The synthesis of Gd_2O_2S: Yb^{3+}, Er^{3+} phosphors was conducted using a solid-state reaction method as described by Kumar et al. (2012) [14]. In this process, stoichiometric amounts of the starting materials, Gadolinium oxide (Gd_2O_3), ytterbium oxide (Yb_2O_3), and erbium oxide (Er_2O_3), were thoroughly mixed. Sulfur was added to the mixture as the sulfur source to form the oxysulfide host lattice. The mixture was then subjected to a two-step calcination process. Initially, it was heated in an air atmosphere at a moderate temperature to promote the formation of an intermediate phase. Subsequently, the temperature was increased, and the atmosphere was changed to one with a controlled amount of sulfur vapor to facilitate the conversion of the intermediate to the final Gd_2O_2S phase. The uniformity of the dopant ions, Yb^{3+} and Er^{3+} was optimized based on the intenisty of the emission under 980 nm wavelength[13]. The detailed conditions and exact temperatures for each step can be found in the cited work [14].

2.2. Measurement and Characterization

For optical thermometry, we employed spectroscopic techniques, such as photoluminescence (PL) spectroscopy, where we excited the phosphor with a 980 nm laser and measured the upconversion emission spectrum. We first measured the room-temperature photoluminescence emission (PL) using an Edinburgh FLS-1000 spectrophotometer equipped with a Continuous Wave (CW) laser.

The upconversion luminescence spectra of the samples were recorded by exciting the sample using the 980 nm line of a continuous-wave laser. The temperature-dependent PL spectra were detected by placing samples inside a chamber (Linkam) in which the temperature was controlled by programmable Fluoracle software. We used the same spectrometer to analyze the luminescence intensity changes as a function of temperature.

Specifically, we sought to identify variations in the ratio of emission intensities from distinct electronic transitions, which

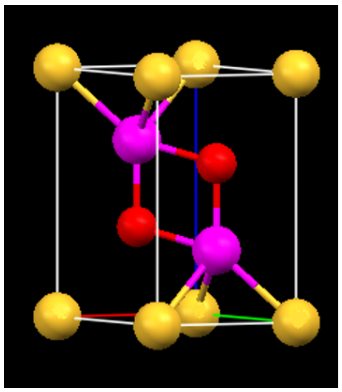

Figure 1: Crystal structure of Gd_2O_2S, illustrating the arrangement of constituent atoms within the unit cell.

are temperature-sensitive and commonly referred to as the fluorescence intensity ratio (FIR) technique. Our focus was on the upconversion luminescence generated from two thermally coupled energy levels and the subsequent non-radiative relaxation process. To minimize variability in measurements, samples were used in powder form, ground using a ball mill, and characterized using an X-ray powder diffractometer (XRD). Figure 1 shows the crystal structure of Gd_2O_2S, and Figure 2 shows the X-ray diffraction pattern for Gd_2O_2S. The symmetry is trigonal, and the space group is P-3m1. There is one formula per unit cell. The structure is very closely related to the A-type rare-earth oxide structure, the difference being that one of the three oxygen sites is occupied by a sulfur atom. Atom positions in Gd_2O_2S using lattice vector units are ± (1/3, 2/3, u) for two metal atoms with u ∼ 0.28, ± (1/3, 2/3, ν) for two oxygen atoms with $\nu \sim 0.63$, and (0, 0, 0) for a sulfur atom. Each metal atom seems to be bonded to four oxygen atoms and three sulfur atoms, to form a seven-coordinated geometry with the oxygen and the metal in the same plane. The XRD results reveal that the well-crystallized Gd_2O_2S: Yb, Er sample is in hexagonal Gd_2O_2S structure with cell parameters a = b = 0.3852 nm, c = 0.6567 nm.

2.3. Data Analysis

Fluorescence Intensity Ratio (FIR), also known as luminescence intensity ratio, is defined as the ratio of two integrated intensities of two separate manifolds m and n [15, 2],

$$\mathrm{FIR} = \frac{\int_{\lambda_{m,1}}^{\lambda_{m,2}} I \, \mathrm{d}\lambda}{\int_{\lambda_{n,1}}^{\lambda_{n,2}} I \, \mathrm{d}\lambda} \, . \tag{1}$$

An alternative definition relies on the ratio of the peak intensities of two manifolds [16],

$$\mathrm{FIR} = \frac{I_1}{I_2} \, . \tag{2}$$

In our analysis, we utilized the photon counts obtained from the FLS1000 spectrometer for a manifold rather than just the peak intensities to calculate the ratio. The former FIR definition has an additional complexity level that comes with inferring

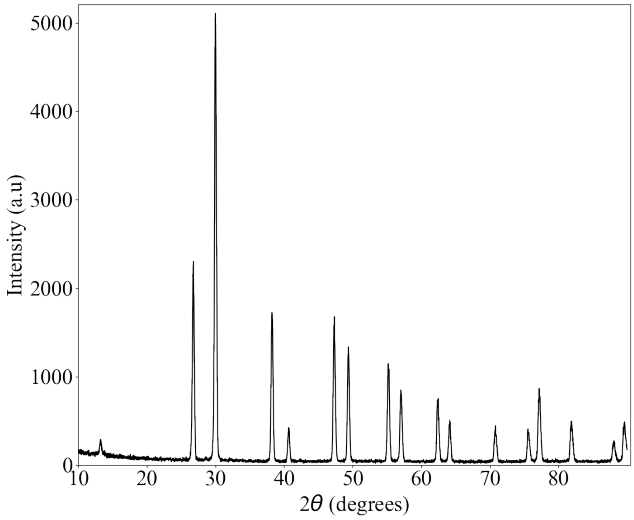

Figure 2: X-ray diffraction (XRD) pattern of Gd_2O_2S where intensity is measured in arbitrary units (a.u.) and θ is the angle of diffraction, confirming the phase purity and crystallographic structure of the synthesized sample, agreeing the space group is P-3m1.

the unknown wavelength ranges of the manifolds $(\lambda_{m,1}, \lambda_{m,2})$, $(\lambda_{n,1}, \lambda_{n,2})$. A common approach to resolving this challenge is to infer these limits through visual inspection of the manifolds empirically. This approach, while offering a practical venue to define and calculate FIR according to Eqn (1), is subject to uncertainties and biases that manifest as misfits of the resulting FIR-temperature relationship to experimental data.

A data-driven approach involves identifying the number of peaks in the manifold, which result from stark splitting of the spectral lines caused by the surrounding electric fields within the lattice. The primary broadening factors for the manifolds need to be identified which are responsible for the creation of the continuous spectral line in the manifold. We can then define each profile corresponding to the peaks as a result of convolution of these broadenings, and can represent the profiles as a function of wavelengths. The final step would be fitting the mixture of these convolutions to the available manifold data.

There are various types of broadening that occur due to different reasons, manifesting as homogeneous and inhomogeneous broadenings. The fitting process could focus on the most dominant broadening. Firstly, inhomogeneous broadening arises from the variation in local crystal field environments and strain. It exhibits a Gaussian profile resulting from the shift in the transition energy of ΔE for an individual ion, which is the sum of numerous small, independent contributions. As expected by the Central Limit Theorem, the distribution of ΔE is Gaussian, where the profile's variance quantifies the spread due to inhomogeneous effects. Secondly, phonon broadening appears to be more dominant over other broadening profiles, particularly as the temperature increases. Phonon broadening, a type of homogeneous broadening, manifests as a Cauchy-Lorentz distribution [17]. Other potential broadening candidates include natural broadening and pressure broadening, which are not as dominant as the two broadenings mentioned above [18, 19, 20, 21]. Therefore, determining the optimal fit for the available data by convolving the mixture of these broadening profiles would be the most effective data-driven approach. However, we defer a comprehensive implementation and application of this data-driven approach to future work where higher-quality experimental data enables its implementation.

The most straightforward approach to inferring the integration limits involves visually inspecting the line spectra at each temperature. A baseline is identified where no peaks are apparent, and the signal is subtracted from the spectral profile. The corrected dataset is then used for analysis. This approach assumes a constant baseline for the entire spectral profile or, at the very least, for the region of interest used for FIR analysis. Baseline correction is an evolving field of research, as baseline shifts can arise from various factors, including stray light within the spectrometer, dark current flowing in the detector, or scattering of residual excitation light. Various methods have been proposed, such as using the Asymmetric Least-Squares Algorithm [22, 23], which appeared to be overkill for the dataset in question.

Once the baseline correction is applied, the integrated intensities for each spectral profile resulting from their respective emissions could be computed. For spectral profiles that appear as a result of transitions from two thermally coupled energy levels to the ground state, there could be significant overlap between these two separate manifolds. Determining a clear boundary between these two manifolds becomes a difficult yet important task, as we would not want to assign one manifold's signal to another. The point in the spectra where the intensity is lowest between the two manifolds for each spectrum is identified and assigned as the boundary between the two manifolds. As for the outer boundaries of the manifolds, they are determined as the wavelength at which the manifolds meet the baseline.

3. Results and Discussion

Figure 3 shows the upconversion emission spectrum of Yb^{3+} Er^{3+} co-doped Gd_2O_2S sample in the wavelength range of 250 - 750 nm at 0° to 600° celsius temperature range. The UC spectrum includes peaks at 524 and 549 nm in the green region, and one band centered at 671 nm in the red region. The former is due to the $^2H_{11/2} \rightarrow ^4I_{15/2}$ and $^4S_{3/2} \rightarrow ^4I_{15/2}$ transitions, and the latter is due to the $^4F_{9/2} \rightarrow ^4I_{15/2}$ transition. Figure 4 shows a possible upconversion mechanism. The two energy levels $^2H_{11/2}$ and $^4S_{3/2}$ are thermally coupled. The dominant green lights peaked at 524 and 549 nm, arising due to the $^2H_{11/2} \rightarrow ^4I_{15/2}$ and $^4S_{3/2} \rightarrow ^4I_{15/2}$ transitions, respectively, which result from the efficient two-photon processes that populate the $^4F_{7/2}$ level and a fast multi-photon non-radiative decay of $^4F_{7/2}$ level to $^2H_{11/2}$ level. Because of several closely spaced levels in between $^2H_{11/2}$ and $^4S_{3/2}$, multi-phonon relaxation results in the decay of the $^2H_{11/2}$ level to $^4S_{3/2}$ yielding the strong emission band at 549 nm. A comparatively weak emission is also observed for the 412 nm band, resulting from

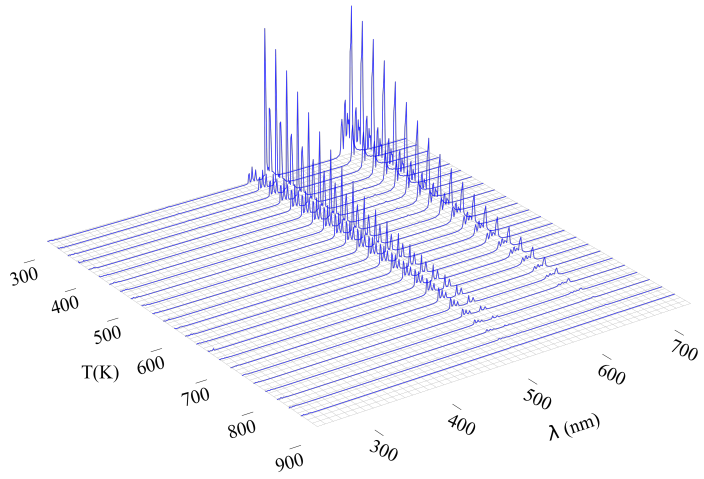

Figure 3: Temperature-dependent emission spectra of Gd_2O_2S presented as a 3D plot, showing variation in photon counts as a function of wavelength (nm) and temperature (K).

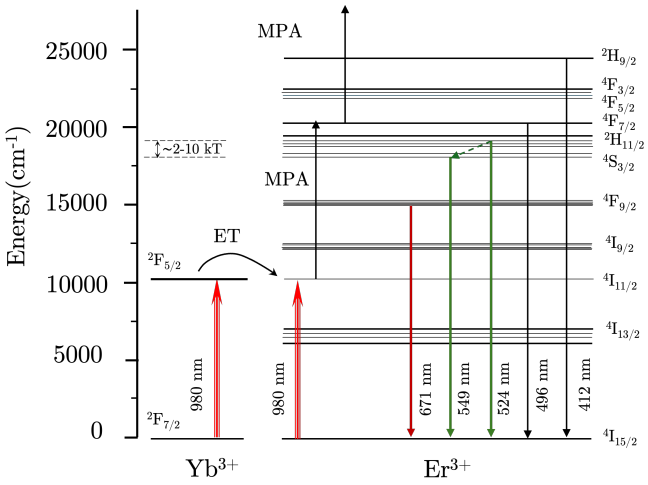

Figure 4: Proposed energy level diagram of Er^{3+} ions, depicting the radiative transitions responsible for the observed emission features.

$^2H_{9/2} \rightarrow ^4 I_{15/2}$ as expected, because the efficiency of the third-order process is less than that of the two-photon process.

Inferring temperature from the available fluorescence intensity is a complex task. The fluorescence intensity from a specific energy level of an ensemble of ions doped in a host material is influenced by various parameters, including the host material, the energy level of interest, the dimensions of the material doped with the ion, and the excitation method employed. By measuring the intensity of fluorescence originating from a specific energy level, the temperature can be theoretically inferred by observing temperature-dependent changes in fluorescence intensity. These changes are usually influenced by various non-radiative rates, such as increased phonon interactions and multi-phonon relaxation, which depend directly on temperature. The intensity of each transition is proportional to the number of atoms (population) in a given excited state at temperature T:

$$I_{1\rightarrow 2} \propto gAh\nu \exp\left(-\frac{E}{K_B T}\right) \tag{3}$$

where, g is the degeneracy of the state, A is the spontaneous emission rate, ν is the frequency, E is the energy of the level, and h and k_B are the Planck constant and Boltzmann constant respectively. The primary challenge associated with employing a single intensity is that any alterations in the excitation intensity, whether attributable to variations in excitation power or excitation wavelength, would be erroneously interpreted as changes in temperature. To circumvent this issue, we can employ a method that involves measuring the intensity of fluorescence from two distinct energy levels that exhibit varying temperature dependencies. This approach provides a self-referencing quantity as a measurand, thereby ensuring that the calibration of the thermometer is entirely independent of the host matrix. This new quantity is defined as Fluorescence Intensity Ratio (FIR). As defined in Eq (1), FIR can be rewritten as follows:

$$\mathrm{FIR} = \frac{\int_{\lambda_{m,1}}^{\lambda_{m,2}} I \, \mathrm{d}\lambda}{\int_{\lambda_{n,1}}^{\lambda_{n,2}} I \, \mathrm{d}\lambda} = \frac{g_1 A_1 h\nu_1}{g_2 A_2 h\nu_2} \exp\left(-\frac{\Delta E_{12}}{K_B T}\right) = B \exp\left(-\frac{\Delta E_{12}}{K_B T}\right) \tag{4}$$

where B is a constant, subscripts 1 and 2 being two distinct energy levels, and ΔE is the energy difference between the two thermally linked levels. We absorb the ratio ν_1/ν_2 into B as they are the frequencies for theoretical transition emission, or the peak of the distribution, which will stay relatively the same even when the temperature changes. Even though energy levels may undergo a slight shift with a temperature change, for our purposes, we assume they remain constant.

The FIR model appears to work best when calculating the ratios of two closely spaced energy levels, often referred to as "thermally coupled" energy levels. Two energy levels are said to be in thermal equilibrium if the separation of energy levels is in the order of a 1-10 kT, where kT ~ 200 cm^{-1} [2, 24]. The ratio of intensities from these energy levels can be understood using the concept of Boltzmann's thermal equilibrium. These empirical limits ensure that the spectral separation is sufficient and the distance is not excessive, thereby allowing for a small exponential temperature decay rate (determined by ΔE). This was proven by our analysis, as shown in Figure 5.

Upconversion processes based on energy transfer, which involve optical pumping, might not seem to follow the Boltzmann distribution at first glance, as it appears that the optical pumping directly influences the population of Stark levels in Er^{3+}. Yet, we can see in Figure 5 that there exists a Boltzmannian relationship for thermally coupled energy levels. For thermally coupled energy levels, due to such a small energy gap, phonon-mediated thermalization occurs in picoseconds whereas the upconversion pumping from Yb^{3+} and radiative decay from the Er^{3+} sublevels occur much slowly in the range of microseconds [13, 25]. As the non-radiative multiphonon transition rates between the cou-

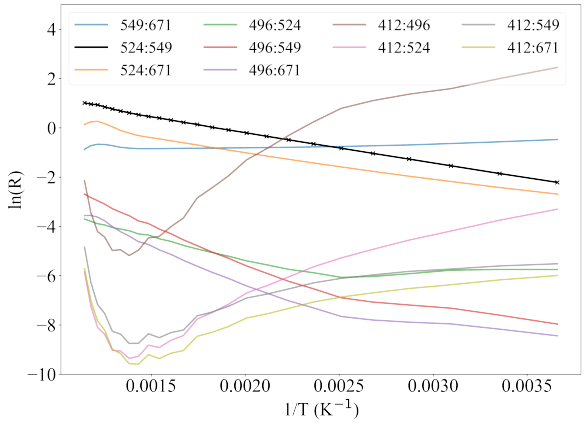

Figure 5: Plot of the natural logarithm of the fluorescence intensity ratio (FIR) as a function of inverse temperature (1/T) for ratios of different emission transitions. Each curve corresponds to a ratio of distinct pair of emission bands, as indicated, highlighting the temperature-dependent behavior of FIR over the measured range and the unique Boltzmannian nature shown by thermally coupled energy levels. Legend uses the peak intensity wavelength for each transition.

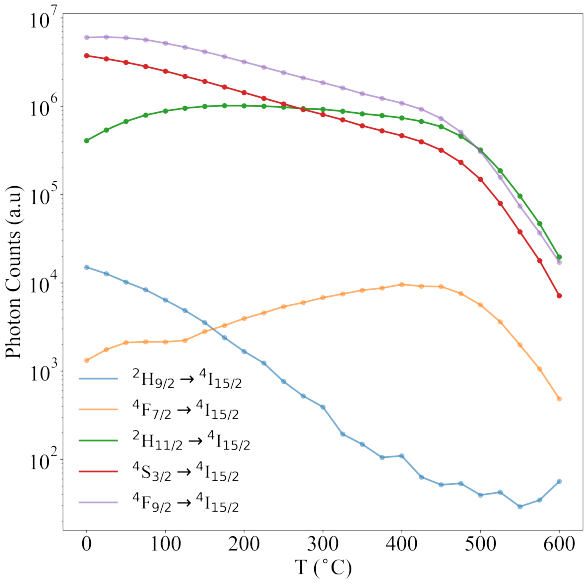

Figure 6: Temperature dependence of the integrated emission intensities of various transitions in Gd_2O_2S. Integrated photon counts are plotted as a function of temperature (°C), with individual transitions indicated in the legend.

pled excited states are substantially higher than the radiative and other competitive relaxation rates, we can assume the distribution followed by thermally coupled energy levels is indeed Boltzmannian in nature, as it will be in a steady state [26].

For our analysis, we chose the ratio of integrated intensities of two thermally equilibrated manifolds with peaks at 524 nm and 549 nm. The ΔE for these two energy levels is $\sim$ 870 cm^{-1}. Figure 6 shows the total integrated intensities for each manifold of emission for Er^{3+} ion in the range of 250 - 750 nm, set in log scale. The bold plots show the change in emission intensity resulting from thermally coupled energy levels, thanks to the phonon contribution between these two energy levels. Even though equation 3 clearly says the intensity has to go down with increasing temperature, we can see that the total photon count for the 524 nm peak actually increases slowly, while the total photon count for the 549 nm peak actually decreases rapidly. This increment in the photon count of the 524 nm peak can be attributed to non-radiative phonon-based energy transfer from the manifold with a peak at 549 nm to the manifold with a peak at 524 nm. Interestingly, the total photon counts for 496 nm peaks, even though they are only in thousands, also increase with increasing temperature, almost mimicking the 524 nm curve. We defer an in-depth investigation of this phenomenon to later publications.

The ratio can be written as

$$\log \mathrm{FIR} = \log \mathrm{B} + \left(\frac{-\Delta E_{12}}{k_B}\right) * \frac{1}{\mathrm{T}} \tag{5}$$

The experimental data are fitted to a straight line with a slope of -1277.6198 and an intercept of 2.3947. The relationship between FIR and temperature can be represented using these values, $\log \mathrm{FIR} = 2.3947 - 1277.6198/\mathrm{T}$. The dependence of FIR on temperature in the range of 0° to 600° celsius is shown in Figure 7a.

The absolute thermal sensitivity indicates how the FIR model responds to changes in temperature. It can be defined as follows:

$$\mathrm{S}_a = \frac{\partial \mathrm{FIR}}{\partial \mathrm{T}} = \mathrm{B}\left(\frac{\Delta \mathrm{E}}{k_B \mathrm{T}^2}\right) \exp\left(\frac{-\Delta \mathrm{E}}{k_B \mathrm{T}}\right) \tag{6}$$

The sensor sensitivity (S_a) for our model is illustrated in Figure 7c. As we can see from the graph, the absolute sensitivity reached the maximum of 0.00459 K^{-1} at the temperature of 573.15 K or 300° celcius. In addition, we utilize another measure of sensitivity known as relative thermal sensitivity, denoted as S_r. S_a is unsuitable for comparing the performance of dissimilar luminescent thermometers because it is influenced by sample characteristics (such as absorption and lifetimes) and the experimental setup. The relative thermal sensitivity S_r, often expressed in units of % change per Kelvin of temperature change (%K^{-1}) or as fractional change per unit of Kelvin (K^{-1}), quantifies the relative change in FIR per degree of temperature change and offers a significant advantage by being independent of the thermometer's nature [2, 27]. It is defined as follows:

$$\mathrm{S}_r = \frac{1}{\mathrm{FIR}} \left|\frac{\partial \mathrm{FIR}}{\partial \mathrm{T}}\right| = \left|\frac{\Delta \mathrm{E}}{k_B \mathrm{T}^2}\right| = \frac{1277.6198}{\mathrm{T}^2} \tag{7}$$

Figure 7d shows the change in relative sensitivity with change in temperature. We multiply the Equation (7) by 100 % if we want to use percentage change per Kelvin. The maximum relative thermal sensitivity was found to be 0.01712 K^{-1}.

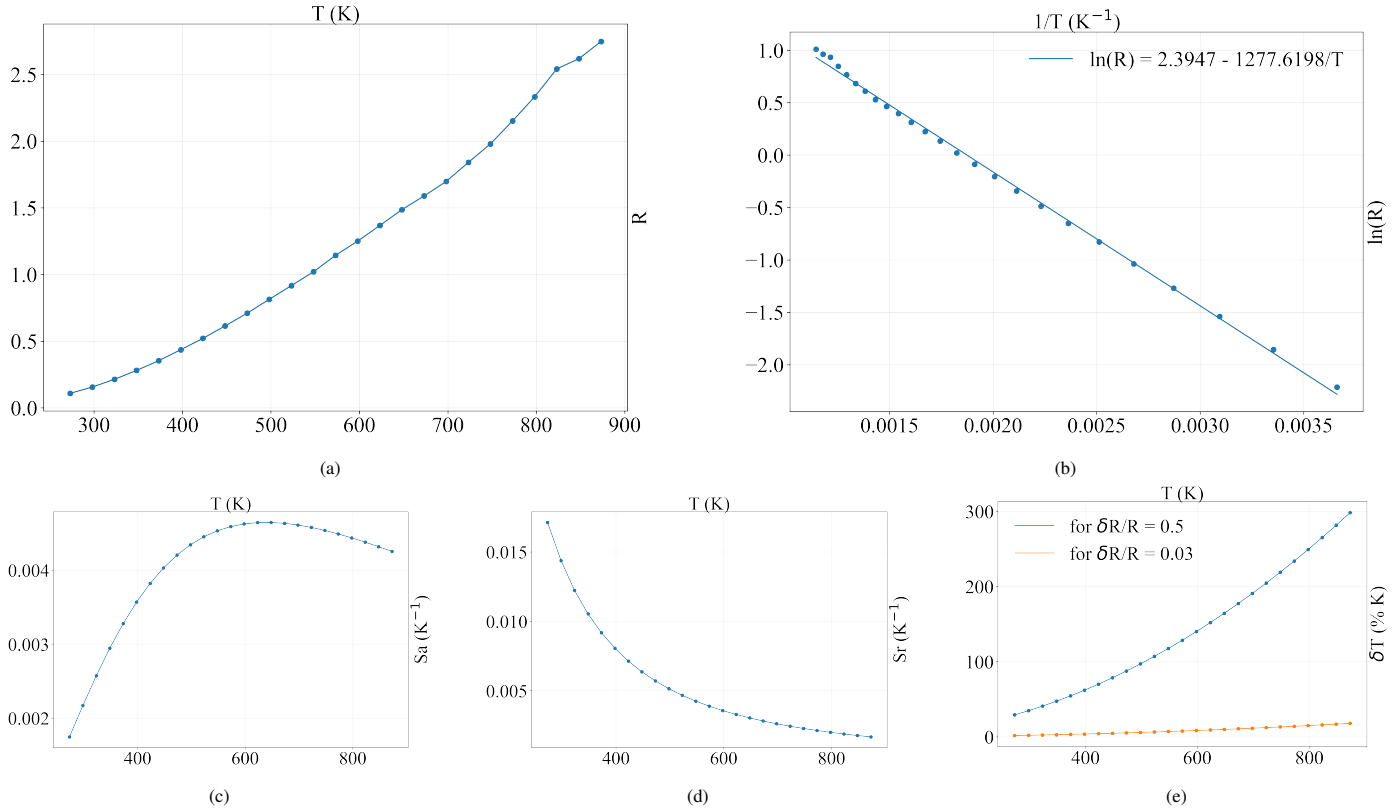

Figure 7: Thermal sensing performance of Gd_2O_2S analyzed through multiple optical thermometry metrics: (a) Fluorescence Intensity Ratio (FIR) as a function of temperature (K), showing the variation in emission behavior with thermal input; (b) logarithm of FIR plotted against inverse temperature (K^{-1}), with a linear fit applied to extract temperature-dependent characteristics; (c) absolute sensitivity (K^{-1}) versus temperature(K), illustrating the material's responsiveness to temperature changes; (d) relative sensitivity (K^{-1}) versus temperature(K), indicating the fractional response per unit temperature; and (e) temperature uncertainty (%K) as a function of temperature, with two trendlines corresponding to different analysis methods, as labeled.

Temperature resolution (also referred to as temperature uncertainty) δT is the smallest temperature change that the luminescent thermometer can detect. A thermometer with high resolution (low uncertainty) is considered to be best for temperature sensors applications [28]. It can be calculated using equation (8)

$$\delta T = \frac{1}{S_r} \frac{\delta FIR}{FIR} \tag{8}$$

where δFIR/FIR is the sensitivity of the detection system. For the PMT device, the sensitivity of the detection system is 0.03 % at maximum SNR operating conditions, but we can use 0.5 % in general scenario. Figure 7e represents the thermal sensitivity in general and maximum SNR condition, where the minimum uncertainty is 1.7520 % K (0.01752 K) at 273.15 K, and the maximum uncertainty is 17.9018 % K (0.1790 K) at 873.15 K for maximum SNR condition. In a general condition, the minimum and maximum uncertainties were found to be 0.29199 K and 2.9836 K, respectively.

4. Conclusions

In this study, we have demonstrated the Gd_2O_2S : 9% Yb^{3+}, 1% Er $^{3+}$ upconversion phosphors as a potential candidate for optical thermometry, leveraging Er^{3+} temperature-dependent luminescence properties for non-contact based temperature sensing. Through detailed spectral analysis, we proposed the mechanisms governing the thermal sensitivity of this phosphor, particularly the fluorescence intensity ratio (FIR) of the thermally coupled $^2H_{11/2} \rightarrow {}^4I_{15/2}$ and $^4S_{3/2} \rightarrow {}^4I_{15/2}$ transitions of Er^{3+} under 980 nm (NIR) excitation. Our results confirm that Gd_2O_2S : Er, Yb phosphors exhibit exceptional thermal sensing capabilities, with reliable performance up to 875 K, making them suitable for high-temperature applications in harsh environments where conventional sensors are impractical.

Our findings show the potential of Gd_2O_2S: 9% Yb^{3+}, 1% Er^{3+} phosphors for applications in different areas such as industrial monitoring, aerospace, and biomedical diagnostics, where high sensitivity and non-invasive sensing are essential. Our work lays the groundwork for the development of next-generation optical thermometers, combining advanced materials with data-driven approaches to address the demands of emerging technological challenges. These results can be further improved with higher-resolution data, enabling the development of a completely

data-driven FIR model minimally affected by uncertainties and biases due to human intervention (e.g., visual inspections) in the FIR model construction.

References

[1] M. L. Phillips, M. P. Hehlen, K. Nguyen, J. M. Sheldon, N. J. Cockroft, Upconversion phosphors: recent advances and new applications, in: Physics and Chemistry of Luminescent Materials: Proceedings of the Eighth International Symposium, Vol. 99 No, 40, The Electrochemical Society, 2000, p. 123.

[2] C. Brites, A. Millán, L. Carlos, Lanthanides in luminescent thermometry, in: Handbook on the physics and chemistry of rare earths, Vol. 49, Elsevier, 2016, pp. 339–427.

[3] L. C. Ong, M. K. Gnanasammandhan, S. Nagarajan, Y. Zhang, Upconversion: road to el dorado of the fluorescence world, Luminescence 25 (4) (2010) 290–293.

[4] M. Pokhrel, D. K. Sardar, et al., High upconversion quantum yield at low pump threshold in er^{3+}/yb^{3+} doped la_2o_2s phosphor, Materials letters (2013).

[5] C. D. Brites, S. Balabhadra, L. D. Carlos, Lanthanide-based thermometers: at the cutting-edge of luminescence thermometry, Advanced Optical Materials 7 (5) (2019) 1801239.

[6] T. Li, C. Guo, S. Zhou, C. Duan, M. Yin, Highly sensitive optical thermometry of yb3+-er3+ codoped agla (moo4) 2 green upconversion phosphor, Journal of the American Ceramic Society 98 (9) (2015) 2812–2816.

[7] M. Abbas, N. Khan, J. Mao, L. Qiu, X. Wei, Y. Chen, S. Khan, Lanthanide and transition metals doped materials for non-contact optical thermometry with promising approaches, Materials Today Chemistry 24 (2022) 100903.

[8] K. Elzbieciak-Piecka, L. Marciniak, Optical heating and luminescence thermometry combined in a cr3+-doped yal3 (bo3) 4, Scientific reports 12 (1) (2022) 16364.

[9] B. Hou, M. Jia, P. Li, G. Liu, Z. Sun, Z. Fu, Multifunctional optical thermometry based on the rare-earth-ions-doped up-/down-conversion ba2tige2o8: Ln (ln= eu3+/er3+/ho3+/yb3+) phosphors, Inorganic Chemistry 58 (12) (2019) 7939–7946.

[10] Y. Yang, C. Mi, F. Yu, X. Su, C. Guo, G. Li, J. Zhang, L. Liu, Y. Liu, X. Li, Optical thermometry based on the upconversion fluorescence from yb3+/er3+ codoped la2o2s phosphor, Ceramics International 40 (7) (2014) 9875–9880.

[11] S. Zhou, K. Deng, X. Wei, G. Jiang, C. Duan, Y. Chen, M. Yin, Upconversion luminescence of nayf4: Yb3+, er3+ for temperature sensing, Optics Communications 291 (2013) 138–142.

[12] M. Haase, H. Schäfer, Upconverting nanoparticles, Angewandte Chemie International Edition 50 (26) (2011) 5808–5829.

[13] M. Pokhrel, G. Kumar, D. Sardar, Highly efficient nir to nir and vis upconversion in er 3+ and yb 3+ doped in m 2 o 2 s (m= gd, la, y), Journal of Materials Chemistry A 1 (38) (2013) 11595–11606.

[14] G. Kumar, M. Pokhrel, A. Martinez, R. Dennis, I. Villegas, D. Sardar, Synthesis and spectroscopy of color tunable y2o2s: yb^{3+}, er^{3+} phosphors with intense emission, Journal of Alloys and Compounds 513 (2012) 559–565.

[15] H. Kusama, O. J. Sovers, T. Yoshioka, Line shift method for phosphor temperature measurements, Japanese Journal of Applied Physics 15 (12) (1976) 2349.

[16] K. Morita, T. Katsumata, S. Komuro, H. Aizawa, Fiber-optic thermometry using thermal radiation from tm end doped sio2 fiber sensor, Review of Scientific Instruments 85 (4) (2014).

[17] A. Jha, S. Shen, M. Naftaly, Structural origin of spectral broadening of 1.5-μm emission in er 3+-doped tellurite glasses, Physical Review B 62 (10) (2000) 6215.

[18] W. Demtröder, Laser spectroscopy, Vol. 2, Springer, 1973.

[19] P. F. Bernath, Spectra of atoms and molecules, Oxford university press, 2020.

[20] M. Fox, Optical properties of solids, Vol. 3, Oxford university press, 2010.

[21] I. B. Gornushkin, L. A. King, B. W. Smith, N. Omenetto, J. D. Winefordner, Line broadening mechanisms in the low pressure laser-induced plasma, Spectrochimica Acta Part B: Atomic Spectroscopy 54 (8) (1999) 1207–1217.

[22] S. He, W. Zhang, L. Liu, Y. Huang, J. He, W. Xie, P. Wu, C. Du, Baseline correction for raman spectra using an improved asymmetric least squares method, Analytical Methods 6 (12) (2014) 4402–4407.

[23] Z.-y. Dong, J.-l. Xu, Baseline estimation using optimized asymmetric least squares (o-als), Measurement 233 (2024) 114731.

[24] S. A. Wade, S. F. Collins, G. W. Baxter, Fluorescence intensity ratio technique for optical fiber point temperature sensing, Journal of Applied physics 94 (8) (2003) 4743–4756.
[25] J. J. Van Hest, G. A. Blab, H. C. Gerritsen, C. de Mello Donega, A. Meijerink, The role of a phonon bottleneck in relaxation processes for ln-doped nayf4 nanocrystals, The Journal of Physical Chemistry C 122 (7) (2018) 3985–3993.
[26] M. Suta, A. Meijerink, A theoretical framework for ratiometric single ion luminescent thermometers—thermodynamic and kinetic guidelines for optimized performance, Advanced Theory and Simulations 3 (12) (2020) 2000176.
[27] X. Yang, Z. Fu, Y. Yang, C. Zhang, Z. Wu, T. Sheng, Optical temperature sensing behavior of high-efficiency upconversion: Er3+–yb3+ co-doped nay (moo4) 2 phosphor, Journal of the American Ceramic Society 98 (8) (2015) 2595–2600.
[28] F. Jahanbazi, Y. Wang, J. A. Dorman, Y. Mao, La2zr2o7: Pr3+ nanoparticles for luminescence thermometry based on a single parameter over a wide temperature range of 620 k, Journal of Alloys and Compounds 911 (2022) 165013.